

Effective Hamiltonian for the electronic properties of the quasi-one-dimensional material $\text{Li}_{0.9}\text{Mo}_6\text{O}_{17}$

Jaime Merino*

*Departamento de Física Teórica de la Materia Condensada and Instituto Nicolás Cabrera,
Universidad Autónoma de Madrid, Madrid E-28049, Spain*

Ross H. McKenzie†

School of Mathematics and Physics, University of Queensland, Brisbane 4072 Queensland, Australia

(Received 25 April 2012; published 18 June 2012)

The title material has a quasi-one-dimensional electronic structure and is of considerable interest because it has a metallic phase with properties different from a simple Fermi liquid, a poorly understood “insulating” phase, and a superconducting phase which may involve spin triplet Cooper pairs. Using the Slater-Koster approach and comparison with published band-structure calculations we present the simplest possible tight-binding model for the electronic band structure near the Fermi energy. This describes a set of ladders with weak (and frustrated) interladder hopping. In the corresponding lattice model the system is actually close to one-quarter filling (i.e., one electron per pair of sites) rather than half-filling, as has often been claimed. We consider the simplest possible effective Hamiltonian that may capture the subtle competition between unconventional superconducting, charge ordered, and non-Fermi liquid metal phases. We argue that this is an extended Hubbard model with long-range Coulomb interactions. Estimates of the relevant values of the parameters in the Hamiltonian are given. Nuclear magnetic resonance relaxation rate experiments should be performed to clarify the role of charge fluctuations in $\text{Li}_{0.9}\text{Mo}_6\text{O}_{17}$ associated with the proximity to a Coulomb driven charge ordering transition.

DOI: [10.1103/PhysRevB.85.235128](https://doi.org/10.1103/PhysRevB.85.235128)

PACS number(s): 71.27.+a, 74.40.Kb, 71.30.+h, 71.45.Lr

I. INTRODUCTION

The electronic properties of quasi-one-dimensional (Q1D) materials are of particular interest because of the possibility that they may exhibit properties characteristic of Luttinger liquid rather than the conventional Fermi liquid metallic state seen in three-dimensional metals. These systems may display Luttinger liquid (LL) behavior above a temperature at which the thermal energy $k_B T$ is larger than the interchain hopping energy t_\perp (Ref. 1). In a LL charge and spin are carried by independent collective excitations instead of the spin-1/2 charged quasiparticles present in a Fermi liquid. Photoemission experiments can probe the existence of a LL through the observation of low-energy spinon and holon branches and a power-law suppression of the density of states at the Fermi energy. Possible realizations of a LL have been investigated extensively in recent years. Examples are the Q1D cuprate materials, SrCuO_2 (Ref. 2) and Sr_2CuO_3 (Ref. 3), Q1D organic crystals,⁴ carbon nanotubes,^{5,6} GaAs channels^{7,8} and more recently one-dimensional Au chains deposited on Ge(001) surfaces.⁹

Apart from the intrinsic interest in finding a LL in actual materials, quasi-one-dimensional materials often exhibit low-temperature broken symmetry states including superconducting, charge and/or spin density waves, and Peierls phases. These instabilities of the metallic phase occur at a crossover temperature scale at which the system effectively becomes three dimensional and so long-range order can occur at low but finite temperatures. The physics associated with this crossover, which goes from the pure one-dimensional to the three-dimensional system as temperature, is reduced and understanding the possible competing ground states at low temperatures remains a formidable theoretical challenge.

Another example of a material which may exhibit one-dimensional physics is the purple bronze $\text{Li}_{0.9}\text{Mo}_6\text{O}_{17}$, which

shows some behavior consistent with a LL¹⁰ at sufficiently high temperatures. Angular-resolved photoemission spectra (ARPES) shows that quasiparticles do not exist in the system since a power-law suppression in the density of states (DOS) is found at the Fermi energy and dispersing spinon and holon branches are seen in the spectral density. At sufficiently low temperatures there is a transition to an insulating-like or semi-conducting state from which superconductivity occurs at even lower temperatures. The low-temperature “insulating” state is poorly understood. The experimental data pose challenging questions to address, apart from the LL behavior observed above the crossover temperature scale. To understand the mechanism of superconductivity it is important to determine the symmetry of the Cooper pairs. It is also important to characterize the “insulating” phase seen below $T_m \sim 25$ K. Finally, it is necessary to characterize the nature of the excitations in the metallic state, in particular, if the material is a “bad metal” with incoherent excitations or not.

Here we introduce a realistic microscopic model on a lattice which can capture the essential physics observed. This model consists of weakly coupled ladders describing the d orbitals in the Mo atoms with strong on-site and off-site Coulomb repulsion. Based on this model we establish that $\text{Li}_{0.9}\text{Mo}_6\text{O}_{17}$ should be regarded as a nearly quarter-filled system and not as a nearly half-filled system. This means that in the absence of longer-range Coulomb interactions the systems would always be a metal. Thus, the finite spatial extension of the Coulomb repulsion should not be neglected and can lead to charge-ordering phenomena and a Wigner-Mott insulator. The model contains rich physics since it contains low dimensionality, strong Coulomb interactions, geometrical frustration, and charge-order frustration. We discuss possible ground states of the proposed model in different limits.

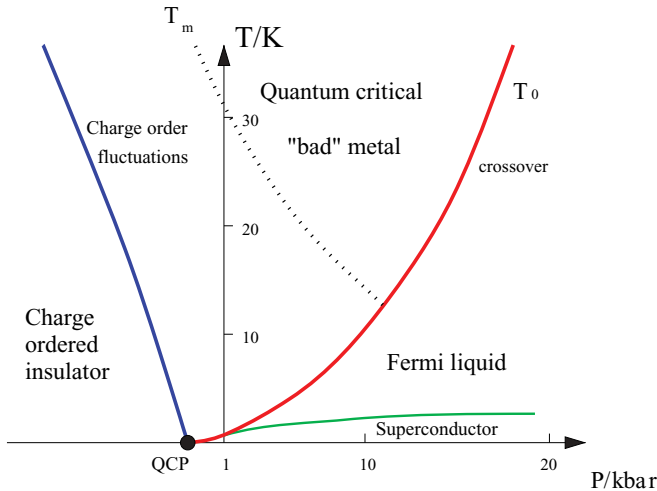


FIG. 1. (Color online) A speculative temperature-pressure phase diagram relevant to $\text{Li}_{0.9}\text{Mo}_6\text{O}_{17}$. It assumes that at ambient pressure the system is close to a quantum critical point for an insulating charge-ordered phase. Fluctuations associated with this phase cause the resistivity to increase with decreasing temperature below T_m . The pressure dependence of this curve is taken from Fig. 3(a) in Ref. 11. Associated with the quantum critical point (QCP) there is a crossover from a quantum critical metal (or “bad” metal) to a Fermi liquid metal at a temperature scale T_0 . The associated coherence temperature goes to zero as the QCP is approached. Similar physics has been observed in recent studies of a two-dimensional extended Hubbard model at one-quarter filling (cf. Fig. 3 in Ref. 12).

From the model proposed, experimental observations, and theoretical considerations we speculate that $\text{Li}_{0.9}\text{Mo}_6\text{O}_{17}$ is close to a quantum critical point dominated by charge-ordering fluctuations. A possible schematic phase diagram is shown in Fig. 1.

The present paper is organized as follows. In Sec. II we briefly revise key experimental observations in $\text{Li}_{0.9}\text{Mo}_6\text{O}_{17}$. In Sec. III we discuss the one-electron tight-binding parameters appropriate for $\text{Li}_{0.9}\text{Mo}_6\text{O}_{17}$ based on a Slater-Koster parametrization and comparison with density functional theory (DFT) calculations of the band structure. Section IV introduces the Coulomb repulsion energies which are relevant for the description of the title material. This leads to a minimal strongly correlated model which consists on weakly coupled ladders comprising the full three-dimensional crystal structure. Finally, in Sec. V we discuss the theoretical implications of the model obtained and possible consequences.

II. BRIEF REVIEW OF EXPERIMENTS

We now review some key observed properties of $\text{Li}_{0.9}\text{Mo}_6\text{O}_{17}$, with a particular emphasis on deviations from the behavior seen in conventional metals and charge-ordered insulators.

A. Electronic anisotropies

Recent measurements of the resistivity along the three crystal axes yielded a resistivity anisotropy of: $\rho_a : \rho_b : \rho_c \simeq 80:1:1600$ at $T = 300$ K and $\rho_a : \rho_b : \rho_c \simeq 150: 1: 1600$ at $T = 4.2$ K (Refs. 13–15). Much smaller anisotropies have

been observed by other authors.^{16,17} However, care must be taken in measuring the conductivity parallel to the chains because it can be reduced significantly if the current path is not strictly parallel to the chains.¹⁵ These are consistent with observed anisotropies in the superconducting upper critical fields.¹³ Hence, these measurements corroborate the quasi-one-dimensionality of the system in its electronic properties.

B. The bad metal

Transport properties of a wide range of strongly correlated electron materials exhibit certain features that are distinctly different from the electronic properties of elemental metals.¹⁸ These unusual properties arise from the emergence of a low-energy scale which defines a temperature scale T_0 (often in the range 10–100 K) above which quasiparticles do not exist and the material is referred to as a bad metal. Signatures of this crossover from a Fermi liquid at low temperature to a bad metal at temperatures above T_0 include (i) the resistivity, Hall coefficient, and thermopower have a nonmonotonic temperature dependence, (ii) with increasing temperature the intralayer resistivity smoothly increases to values much larger than the Mott-Ioffe-Regel limit ($\hbar^2 a/e \sim 1 \text{ m}\Omega\text{cm}$) corresponding to a mean-free path comparable to the lattice constant a (Ref. 19), (iii) at temperatures of order T_0 the thermopower has values as large as $k_B/e \sim 80 \mu\text{V/K}$, and (iv) above T_0 the Drude peak in the frequency-dependent conductivity collapses and the associated spectral weight shifts to higher frequencies.

It is important to realize that if quasiparticles do not exist then the one-electron spectral function does not have dispersive features (i.e., it is completely incoherent). This means that above T_0 the notion of a band structure and a Fermi surface have no meaning. All of the above features in the transport are captured by a dynamical mean-field theory (DMFT) treatment of lattice Hamiltonians such as the Hubbard model and Anderson lattice model.¹⁸ It is generally believed that a small T_0 is associated with proximity to a Mott insulator or to a quantum critical point.¹² An alternative picture of bad metals can be given in terms of hard core bosons.²⁰

$\text{Li}_{0.9}\text{Mo}_6\text{O}_{17}$ exhibits many of the above signatures of bad metallic behavior.

1. Resistivity

The magnitude of the resistivity parallel to the chains is about $100 \mu\Omega\text{cm}$ at 100 K (Refs. 14 and 15). This is comparable to that observed in other “bad metals” such as optimally doped cuprate superconductors.^{19,21} For a double chain, the conductivity can be written as $\sigma_b = 4e^2 \ell_b / [\pi(ac)\hbar]$ where ℓ_b is the mean-free path along the chains and a and c are the unit cell dimensions perpendicular to the chain direction. This leads to an estimate $\ell_b \sim 5 - 7 \text{ \AA}$, using the experimental resistivities $\rho_b \sim 300\text{--}400 \mu\Omega\text{cm}$ at 300 K. This estimate suggests that at $T = 300$ K the material is at the Mott-Ioffe-Regel limit.

2. Thermoelectric power

The thermopower is positive in sign and a nonmonotonic function of temperature, increasing from a value of approximately $20 \mu\text{V/K}$ at low temperatures to a maximum of

about $30 \mu\text{V/K}$ at 50 K and then decreasing slowly to a value of about $10 \mu\text{V/K}$ around room temperature.²² Recent measurements²³ found that the magnitude of the thermopower exhibited a significant sample dependence, with values as large as $200 \mu\text{V/K}$, and was interpreted in terms of bipolar transport in an almost perfectly compensated metal. All of the above behavior contrasts to what was observed in a simple Fermi liquid in which the thermopower was approximately linear in temperature for temperatures less than T_0 (Ref. 24). Furthermore, in contrast to experiments, the band structure suggests that the thermopower should be negative since the system has an electron-like Fermi surface, with two bands close to one-quarter filling.

3. Frequency-dependent conductivity

The optical conductivity at both 10 and 300 K is relatively flat as a function of frequencies of the scale of tens of millielectronvolts,²⁵ suggesting the absence of a Drude peak. The total spectral weight at low frequencies is quite small, corresponding to about one charge carrier per ten unit cells if one integrates up to about 0.1 eV. For electric field polarizations perpendicular to the chain direction there is a clear energy gap of about 0.4 eV, at both 10 and 300 K. Hence, the material has the very unusual property that it appears to be conducting for transport parallel to the chains and insulating for transport perpendicular to the chains.

4. Hall effect

The transverse conductivity σ_{ab} increases by a factor of about 60 as the temperature decreases from 300 to 25 K (Ref. 15). The Hall coefficient increases by several orders of magnitude from $(1-3) \times 10^{-9} \text{ m}^3/\text{C}$ to about $10^{-6} \text{ m}^3/\text{C}$ as temperature decreases from 200 to 2 K (Refs. 16 and 23). This is inconsistent with a simple Fermi liquid metal in which the Hall coefficient should be independent of temperature. The value obtained for $\text{Li}_{0.9}\text{MoO}_6\text{O}_{17}$ assuming a Drude model $R_H = -1/n|e|$ is $R_H \sim -2 \times 10^{-9} \text{ m}^3/\text{C}$, assuming $n = 1.9$ electron charge carriers per unit cell. This value is consistent with the absolute experimental value at $T = 250$ K although with the opposite sign.²⁶ The T dependence of R_H shares some similarities with the observed behavior in the organic charge transfer salt tetramethyltetrafulvalene (TMTTF)₂AsF₆. In this material, the Hall coefficient increases by a factor of about 100 as the temperature decreases from 200 to 100 K, at which there is a charge-ordering transition.²⁷ The Hall coefficient has been calculated for a set of weakly coupled Luttinger liquids with umklapp scattering associated with one-half filling.²⁸ Similar results are expected near one-quarter filling. There are small power-law temperature-dependent corrections to the high temperature noninteracting value. The bandwidth sets the scale for this temperature dependence. In summary, the Hall effect is inconsistent with both a quasi-1D Fermi liquid and a Luttinger liquid picture even at the qualitative level.

5. Thermal conductivity

The Lorenz ratio is about 10 to 30 times the Fermi liquid value, implying a gross violation of the Wiedemann-Franz law.¹⁵ This has been interpreted in terms of a Luttinger liquid picture with spin-charge separation. The Hall Lorenz ratio

increases from about 100 to 10^5 times the Fermi liquid value as the temperature decreases from 300 to 25 K (Ref. 15).

6. Angle-resolved photoemission spectroscopy

This measures the one-electron spectral density and results^{10,29} have been interpreted in terms of Luttinger liquid and non-Fermi liquid pictures. The characteristic features in the spectral function of LL's have been theoretically obtained previously.^{30,31} The ARPES data display characteristic holon and spinon branches as well as the characteristic suppression of the single particle density of states (DOS) of a one-dimensional system signaling the destruction of quasiparticles and of Fermi liquid behavior. However, the exponent α characterizing the DOS suppression depends on T varying between $\alpha \approx 0.6$ for $T \leq 200\text{K}$ and $\alpha \approx 0.9$ at $T = 300\text{K}$ in contrast with the T -independent α in a one band Luttinger liquid and has been attributed to renormalization of α due to interaction of charge neutral critical modes associated with the two bands crossing the Fermi energy. The scaling of the spectral density with temperature $A(\mathbf{k}, \omega) = T^\eta \bar{A}(v\mathbf{k}/T, \omega/T)$, violates the one-band LL scaling relation $\eta = (\alpha - 1)$ since experimentally $\eta = 0.56$ instead of $\eta < 0$. This unconventional quantum critical scaling indicates the presence of quantum fluctuations which can mask the pure LL behavior. Interestingly no warping of the Fermi surface has been observed in ARPES yet. LL behavior has also been observed in scanning tunneling spectroscopy data³² with $\alpha \approx 0.62$ consistent with ARPES.

7. Nernst effect

Recent measurements have been interpreted in terms of bipolar transport in an almost perfectly compensated metal with close to equal numbers of electrons and holes.²³ The magnitude of the Nernst signal is four orders of magnitude larger than the value given by Behnia's simple Fermi liquid expression.³³

8. Magnetoresistance

This exhibits a number of unusual properties for all temperatures.^{14,16} For magnetic fields parallel to the chains there is a small negative magnetoresistance for all current directions, suggesting the suppression of the "insulating" state. For magnetic fields and currents both perpendicular to the layers (the c -axis direction) there is a huge positive magnetoresistance. At fields of 10 T it can be as large as 50- and 500-fold at temperatures of 50 and 3 K, respectively.¹⁶ This is nonclassical as there is no Lorentz force since the magnetic field and electric current are parallel. Similarly, unusual behavior has also been seen in a wide range of other strongly correlated low-dimensional metals.

C. The "insulating" state

Some properties suggest the possibility of an insulating or semiconducting-like phase at low temperatures. However, it should be stressed that one does not see activated behaviour (i.e., clear evidence for an energy gap). It is observed that the resistivity is a decreasing function of temperature from the superconducting transition temperature $T_c \sim 1$ K up to about 20 K. The resistivity then increases approximately linear with

increasing temperature up to room temperature. The simplest possible explanation would be that there is a metal-insulator transition around 20 K. However, this is inconsistent with several experiments we discuss below. First, the minimum in the resistivity occurs at T_m at different temperatures for different current directions, ranging from $15\text{K} \leq T_{\min} \leq 30\text{K}$. Increasing the pressure to 20 kbar T_m decreases from about 30 to 10 K (Fig. 1), and the magnitude of the resistivity decreases significantly.¹¹ Hence, it is not clear that the “insulating” state exists at high pressures. We also note that high magnetic fields parallel to the chain direction reduce the low-temperature resistivity, which can be interpreted as a destruction of the “insulating” state.¹⁴

The fact that the resistivity is a decreasing function of temperature above the superconducting transition is rather unusual and puzzling since one normally sees a direct transition from a metallic phase to a superconducting phase. However, there are other cases involving quarter-filled organic charge transfer salts where a superconducting state occurs close to a charge-ordered insulator [see the table in Ref. 34 and the inset of Fig. 2 in Ref. 35]. Other quasi-one-dimensional materials exhibit a resistivity with a similar temperature and pressure dependence similar to that summarized in Fig. 1. For example, $\text{Per}_2\text{M}(\text{mnt})_2$ [$\text{M} = \text{Pt}, \text{Au}$] is a charge density wave (CDW) insulator at ambient pressure, but above 0.5 GPa the resistivity has a nonmonotonic temperature dependence.³⁶

An important question is whether the “insulating” state is a CDW driven by a Fermi surface instability with a partially gapped Fermi surface. Such CDWs are observed in other quasi-two-dimensional materials such as $\text{K}_{0.3}\text{MoO}_3$ and the transition-metal dicalchogenide compound 2H-NbSe_2 (Ref. 37). The structural instabilities associated with the CDW can be clearly seen in x-ray scattering. However, high resolution x-ray scattering, neutron scattering,³⁸ and thermal expansion³⁹ experiments on $\text{Li}_{0.9}\text{Mo}_6\text{O}_{17}$ observed no structural instability such as one would expect to be associated with charge-ordering phenomena. However, observing a structural instability driven by Fermi surface nesting requires a sufficiently large electron-lattice coupling which may not be present. Other Mo compounds, such as the blue bronze $\text{K}_{0.3}\text{MoO}_3$ which is quasi-two-dimensional, show jumps in resistivity typical of a more conventional CDW accompanied by a Peierls transition. A possible interpretation of the observations in $\text{Li}_{0.9}\text{Mo}_6\text{O}_{17}$ is that an unconventional electronically driven CDW occurs which is not detectable with structural analysis data. For example, the “insulating” state may be a D -density wave (DDW) state, which has nodes in the energy gap. Such a state has been proposed as the low-temperature state of α -bisethylenedithio-tetrathiafulvalene (BEDT-TTF) $_2\text{KHg}(\text{SCN})_4$ (Ref. 40) and of the pseudogap state in the cuprates.⁴¹ Since in a DDW state there is no modulation of the charge density in real space it is hard to detect the associated symmetry breaking or long-range order.

It is important to determine the possible nature of the magnetic interactions if they exist in the “insulating” phase. The temperature dependence of the magnetic susceptibility has a Curie contribution from a small number of magnetic impurities (about 10^{-4} per conduction electron).⁴² Subtracting the Curie contribution, the remainder is weakly temperature dependent, between about 10 and 200 K, characteristic of the

Pauli paramagnetism of a Fermi liquid metal. Hence, there is no sign of the energy gap that is normally seen in CDWs and charge-ordered insulators. Pauli susceptibility data¹³ lead to $\chi(0) \simeq 2.8 \times 10^{-6}$, consistent with previous data.⁴² At low temperatures the specific heat capacity has a term that is approximately linear in temperature with a coefficient $\gamma \simeq 6 \text{ mJ}/(\text{mol K}^2)$ (Refs. 42 and 43). More recent data find that the specific heat coefficient at temperatures right above the superconducting transition temperature is $\gamma \simeq 1.6 \text{ mJ}/(\text{mol K}^2)$. From the Fermi velocity obtained from band-structure calculations⁴⁴ $\hbar v_F = 3.7 \text{ eV}\text{\AA}$, one finds a bare density of states at the Fermi energy due to the two $\text{Mo}(d_{xy})$ one-dimensional bands $D(\epsilon_F) = 1.9 \text{ states}/(\text{eV cell})$. This unrenormalized bare DOS is three times larger than the DOS obtained from the experimental¹³ specific heat slope $\gamma \simeq 1.6 \text{ mJ}/\text{mol K}^2$.

Experimental data lead to a Sommerfeld-Wilson ratio⁴⁵ $R \equiv 4\pi^2 k_B^2 \chi(0)/[3(g\mu_B)^2 \gamma] \approx 2$, indicating substantial electronic correlation effects.¹³

The fact that the charge transport properties (resistivity and the Hall coefficient) show “insulating” behavior with decreasing temperature while the thermodynamic properties (specific heat and magnetic susceptibility) show Fermi liquid properties is puzzling. One possible explanation is that the second case is associated with low-energy spin excitations and not charge excitations.

D. Superconducting state

The transition temperature T_c can vary between about 1 to 2 K depending on sample purity. Substituting Li ions with K and Na ions led to a reduction in T_c and a correlation between T_c with the residual resistivity.⁴² Such a sensitivity is characteristic of an unconventional superconductor (i.e., non- s -wave pairing).⁴⁶ Increasing the pressure to 20 kbar T_c increases from about 1.8 to 2.5 K (Ref. 11). The upper critical field for magnetic fields parallel to the chains may be above the Chandrasekhar-Clogston-Pauli paramagnetic limit for a spin singlet superconductor¹³ suggesting the possibility of a spin triplet state.

E. Isoelectronic materials

It might be expected that the materials $\text{A}_{0.9}\text{Mo}_6\text{O}_{17}$ with the alkali metals $\text{A} = \text{K}, \text{Na}, \text{Tl}$ have similar properties and much can be learned from comparisons to $\text{A} = \text{Li}$. However, it turns out that these materials have a slightly different crystal structure, with separated metal-oxygen layers leading to a significantly different electronic structure.⁴⁷ Specifically, they turn out to have three partially filled d -block bands and a quasi-two-dimensional band structure and Fermi surface. They undergo CDW instabilities due to a hidden Fermi surface nesting.⁴⁸ For $\text{A} = \text{K}$ the CDW transition occurs at 120 K, associated with a structural transition increasing the unit cell dimensions four fold, as seen by x-ray scattering and electron diffraction.⁴⁹ At the transition about 50 percent of the charge carriers are gapped out. For $\text{A} = \text{Na}$ the CDW transition occurs at 80 K, and the opening of the energy gap on two of the bands crossing the Fermi energy has been seen in angle-resolved photoemission spectroscopy (ARPES).⁵⁰

III. TIGHT-BINDING BAND STRUCTURE

To introduce the simplest strongly correlated model to describe the electronic properties of $\text{Li}_{0.9}\text{MoO}_6\text{O}_{17}$, we first analyze the band structure published earlier using the extended Hückel method⁵¹ and the local density approximation (LDA) version of DFT.⁴⁴

These calculations allow extracting the nominal valence of the compound, $\text{LiMo}_6\text{O}_{17}$. The band structure shows the existence of two d_{xy} bands crossing the Fermi energy and two d_{xz}/d_{yz} bands which are filled with two electrons leading to six electrons in the unit cell. The d_{xz} and d_{yz} bands are shifted away from the d_{xy} bands and the Fermi energy becoming completely filled due to hybridization with the neighboring O atoms. This effectively leads to two isolated d_{xy} bands crossing the Fermi energy which contain two electrons. Since there are four Mo atoms per unit cell, this implies that each Mo chain atom has 1.5 electrons with one electron in the d_{xz}/d_{yz} orbitals and half an electron in the d_{xy} orbitals. This corresponds to a chemical valence for $\text{LiMo}_6\text{O}_{17}$ of $\text{Li}^{+1}(\text{Mo}^{4.5+})_2(\text{Mo}'^{6+})_4(\text{O}^{2-})_{17}$ where Mo' denote atoms which are not in the conducting zig-zag chains. On the other hand, the doped compound $\text{Li}^{+0.9}(\text{Mo}^{4.55+})_2(\text{Mo}'^{6+})_4(\text{O}^{2-})_{17}$, has the Mo orbital with suppressed electron density $\text{Mo}(4d^{1.45})$ so that there are less than 0.5 electrons (about 0.45) per d_{xy} orbital of Mo.

A. Slater-Koster parameters

We parametrize the model using the Slater-Koster tight-binding approach.^{52,53} We use $2p_x, 2p_y, 2p_z$ orbitals as the minimum basis set for describing O and $4d_{xy}$ orbitals for describing Mo. Using distances obtained from the x-ray crystal structure⁵⁴ we analyze the hopping amplitudes between Mo and O atoms and the direct hopping amplitudes between the Mo atoms. In a second stage, we single out the important hopping amplitudes needed for an effective tight-binding model Hamiltonian describing the d_{xy} orbitals of Mo.

The distances and displacement vectors needed to define the cosines between the various atoms are shown in Tables I and II together with estimated hopping amplitudes obtained from the Slater-Koster approach. The hoppings between the Mo and O atoms are given by

$$\begin{aligned} t_{p_x d_{xy}} &= m(\sqrt{3}l^2 V_{pd\sigma} + (1 - 2l^2)V_{pd\pi}), \\ t_{p_y d_{xy}} &= l(\sqrt{3}m^2 V_{pd\sigma} + (1 - 2m^2)V_{pd\pi}), \\ t_{p_z d_{xy}} &= lmn(\sqrt{3}V_{pd\sigma} - 2V_{pd\pi}), \end{aligned} \quad (1)$$

TABLE I. Position vectors of the four partially filled Mo atoms (Ref. 54) inside the unit cell of $\text{Li}_{0.9}\text{Mo}_6\text{O}_{17}$ in units of the monoclinic a , b , and c unit cell vectors ($a = 12.762 \text{ \AA}$, $b = 5.523 \text{ \AA}$, and $c = 9.499 \text{ \AA}$). The angle between the a and c axes of the monoclinic crystal is $\beta = 90.61^\circ$.

Mo_i	$(R_{\text{Mo}_i})a$	$(R_{\text{Mo}_i})b$	$(R_{\text{Mo}_i})c$
Mo_1	0.9939	0.25	0.23356
Mo_4	0.16635	0.25	0.9206
Mo'_1	0.00613	0.75	0.7664
Mo'_4	0.8337	0.75	0.07938

TABLE II. Distances between Mo and O atoms (Ref. 54) and hopping amplitudes in $\text{Li}_{0.9}\text{Mo}_6\text{O}_{17}$. Hoppings are estimated based on the Slater-Koster approach. The most relevant nearest-neighbor Mo–Mo and Mo–O distances within the main ladder and between different ladders are displayed. Hopping amplitudes are between $4d_{xy}$ orbitals Mo atoms and between $4d_{xy}$ and $2p_y$ orbitals for Mo–O within a chain. Distances are given in angstrom and hopping in electronvolts. The labeling of the atoms follows Ref. 54 (see Fig. 2).

Atom-atom	Distance (\AA)	Hopping (eV)
$\text{Mo}_1\text{--Mo}'_4$ (in-chain)	3.725	0.1606
$\text{Mo}_1\text{--O}_{11}$ (in-chain)	1.873	1.515
$\text{Mo}_1\text{--Mo}_4$ (interchain)	3.6756	0.
$\text{Mo}_1\text{--O}_1$ (interchain)	1.873	0.
$\text{Mo}_1\text{--Mo}'_1$ (interladder)	5.7655	0.018

where l, m, n are the direction cosines of the vector from the p orbital to the d orbital and the parameters

$$\begin{aligned} V_{pd\sigma} &= -\frac{29.5 \text{ eV}}{d_{\text{MoO}}^{7/2}}, \\ V_{pd\pi} &= \frac{13.6 \text{ eV}}{d_{\text{MoO}}^{7/2}}, \end{aligned} \quad (2)$$

where the distances are in \AA and the parameters are appropriate for Mo. According to the above equations one finds that only the $t_{p_y d_{xy}}$ hopping amplitude between Mo and O atoms in a chain is nonzero and the corresponding value is shown in Table II. Also the hopping amplitude between different chains in a ladder through an O atom is zero with the Slater-Koster approach. The direct hopping between two d_{xy} orbitals maybe estimated from

$$t_{d_{xy}d_{xy}} = 3l^2 m^2 V_{dd\sigma} + (l^2 + m^2 - 4l^2 m^2)V_{dd\pi} \quad (3)$$

with the corresponding parameters

$$\begin{aligned} V_{dd\sigma} &= -\frac{213.3 \text{ eV}}{d_{\text{MoMo}}^5}, \\ V_{dd\pi} &= \frac{115.2 \text{ eV}}{d_{\text{MoMo}}^5}, \end{aligned} \quad (4)$$

where again the distances are all in \AA . The nearest-neighbor intrachain hopping between Mo is then $t_{\text{Mo}_1\text{Mo}'_4} = V_{dd\pi}$ at a distance $d = 3.725 \text{ \AA}$ and between Mo atoms at $d = 3.69 \text{ \AA}$ in different chains $t_{\text{Mo}_1\text{Mo}_4} = V_{dd\sigma} = 0$ (Ref. 53). The hopping amplitude between Mo atoms on different ladders is nonnegligible $t_{\text{Mo}_1\text{Mo}'_1} = V_{dd\pi} = 0.018 \text{ eV}$.

The largest contribution to the interaction between neighboring Mo atoms in the chain comes from hopping through intermediate O atoms. A straightforward estimate of this hopping amplitude from perturbation theory gives

$$t(\text{Mo--Mo}) = \frac{t_{p_y d_{xy}}^2}{\epsilon_{\text{Mo}} - \epsilon_{\text{O}}} = 0.9 \text{ eV}, \quad (5)$$

which leads to a half-bandwidth of 1.8 eV for the chain, a value which is large compared to the LDA-DFT value of about 0.9–1 eV (Ref. 44). Such a discrepancy may be related to the breakdown of the perturbative form since

$|\epsilon_{\text{Mo}} - \epsilon_{\text{O}}| \sim t_{p,d_{xy}}$ using the values $\epsilon_{\text{Mo}}(4d) = -11.56$ eV and $\epsilon_{\text{O}}(2p) = -14.13$ eV. We will discuss in more detail below how the effective nearest-neighbor hopping between Mo atoms needs to be reduced by a factor of two with respect to the Slater-Koster hoppings to correctly reproduce the LDA-DFT bandwidths.

From the Slater-Koster analysis above we would arrive at the conclusion that the zig-zag Mo chains are then decoupled and only a nonzero interladder hopping exists. However, DFT band-structure calculations do indicate the existence of interchain hopping which is, however, much weaker than the effective in-chain hopping. This is because the direct $\text{Mo}_1\text{-Mo}'_4$ bonding in the chain is essentially of the π type whereas the interchain $\text{Mo}_1\text{-Mo}_4$ bond is of the weak δ type since the chains are on top of each other. Therefore, the interchain coupling should come from the small δ -type coupling between the d_{xy} orbitals of the Mo atoms. Ladders are coupled through a direct hopping connecting Mo d_{xy} orbitals. The interladder $\text{Mo}_1\text{-Mo}'_1$ bonding is of the π type. On the other hand, hopping processes via two intermediate O atoms should be very small. This is because one of these intermediate oxygens is an apical O, (O_4 in Fig. 2 of Ref. 54) weakly hybridized to Mo_1 via the O_4 and O'_8 p orbitals. It is important to note that interchain and interladder hoppings should be nonzero to recover the dispersion along the c direction found in DFT calculations. A three-parameter Slater-Koster approach⁵³ to the bands would lead to an interchain hopping amplitude $t_{\text{Mo}_1\text{Mo}_4} = V_{dd\delta} = V_{dd\sigma}/6 = -0.046$ eV which has the opposite sign to the π type of bond between different ladders $t_{\text{Mo}_1\text{Mo}'_1} = 0.018$ eV. We will see below how the opposite signs between these two hopping amplitudes are important in a tight-binding model to capture the LDA-DFT band structure close to the Fermi energy.

B. Effective tight-binding model for $\text{Li}_{0.9}\text{Mo}_6\text{O}_{17}$

We have performed a tight-binding calculation in which we include the four d_{xy} orbitals of the Mo atoms and integrate out the O atoms which are assumed to enter indirectly via the Mo-Mo hopping amplitudes. We keep the most relevant hopping amplitudes needed for the description of the band structure. The simple tight-binding model for the d_{xy} orbitals is compared to previous⁴⁴ and more recent⁵⁵ LDA-DFT band-structure calculations from which the hopping amplitudes can be extracted.

The position of the atoms in the unit cell are expressed as $\mathbf{R}_i = (R_{\text{Mo}_i})_a \mathbf{a} + (R_{\text{Mo}_i})_b \mathbf{b} + (R_{\text{Mo}_i})_c \mathbf{c}$ and the momentum wave vector $\mathbf{k} = k_a \mathbf{a}^* + k_b \mathbf{b}^* + k_c \mathbf{c}^*$, all referred to the unit cell coordinate system. A translation vector of the lattice reads $\mathbf{R}_n = n_a \mathbf{a} + n_b \mathbf{b} + n_c \mathbf{c}$ and the Bloch functions

$$|\Psi_{\text{Mo}_i}(\mathbf{k})\rangle = \frac{1}{\sqrt{N}} \sum_{\mathbf{R}_n} e^{i\mathbf{k}\cdot(\mathbf{R}_n + \mathbf{R}_{\text{Mo}_i})} |\Psi_{\text{Mo}_i}(\mathbf{r} - \mathbf{R}_n - \mathbf{R}_{\text{Mo}_i})\rangle \quad (6)$$

For the effective in-chain interaction we have

$$\begin{aligned} \langle \Psi_{\text{Mo}_1}(\mathbf{k}) | H | \Psi_{\text{Mo}'_4}(\mathbf{k}) \rangle &= \langle \Psi_{\text{Mo}_4}(\mathbf{k}) | H | \Psi_{\text{Mo}'_1}(\mathbf{k}) \rangle \\ &= -2t A(k_a, k_c) \cos\left(\frac{\mathbf{k} \cdot \mathbf{b}}{2}\right), \end{aligned} \quad (7)$$

where $A(k_a, k_c) = e^{i2\pi[k_a(R_{\text{Mo}'_4} - R_{\text{Mo}_1})_a + k_c(R_{\text{Mo}'_4} - R_{\text{Mo}_1})_c]}$. The interaction between chains in the same ladder is described through matrix elements as

$$\begin{aligned} \langle \Psi_{\text{Mo}_1}(\mathbf{k}) | H | \Psi_{\text{Mo}_4}(\mathbf{k}) \rangle &= -t_{\perp} e^{i\mathbf{k}\cdot(\mathbf{a}-\mathbf{c})} e^{i\mathbf{k}\cdot(\mathbf{R}_{\text{Mo}_4} - \mathbf{R}_{\text{Mo}_1})} \\ &= -t_{\perp} e^{i\mathbf{k}\cdot\delta_{\perp}} \end{aligned} \quad (8)$$

where $\delta_{\perp} = 0.17\mathbf{a} - 0.31\mathbf{c}$, and similarly for the $\text{Mo}'_4\text{-Mo}'_1$ interaction

$$\begin{aligned} \langle \Psi_{\text{Mo}'_1}(\mathbf{k}) | H | \Psi_{\text{Mo}'_4}(\mathbf{k}) \rangle &= -t'_{\perp} e^{-i\mathbf{k}\cdot\delta_{\perp}} \\ &= \langle \Psi_{\text{Mo}_1}(\mathbf{k}) | H | \Psi_{\text{Mo}_4}(\mathbf{k}) \rangle^*. \end{aligned} \quad (9)$$

Two ladders in two neighboring unit cells are coupled through the matrix element

$$\begin{aligned} \langle \Psi_{\text{Mo}_1}(\mathbf{k}) | H | \Psi_{\text{Mo}'_1}(\mathbf{k}) \rangle &= -t' e^{i\mathbf{k}\cdot\mathbf{a}} e^{i\mathbf{k}\cdot(\mathbf{R}_{\text{Mo}'_1} - \mathbf{R}_{\text{Mo}_1})} - t' e^{i\mathbf{k}\cdot(\mathbf{a}-\mathbf{b})} e^{i\mathbf{k}\cdot(\mathbf{R}_{\text{Mo}'_1} - \mathbf{R}_{\text{Mo}_1})} \\ &= -2t' e^{i\mathbf{k}\cdot\delta_1} \cos\left(\frac{\mathbf{k} \cdot \mathbf{b}}{2}\right) \end{aligned} \quad (10)$$

where $\delta_1 \equiv \mathbf{a} - \mathbf{b}/2 + \mathbf{R}_{\text{Mo}'_1} - \mathbf{R}_{\text{Mo}_1} = 0.01\mathbf{a} + 0.53\mathbf{c}$. On the other hand, the $\text{Mo}_4\text{-Mo}'_4$ hopping amplitude between ladders is weaker since they are at a larger distance and is neglected

$$\langle \Psi_{\text{Mo}_4}(\mathbf{k}) | H | \Psi_{\text{Mo}'_4}(\mathbf{k}) \rangle = 0. \quad (11)$$

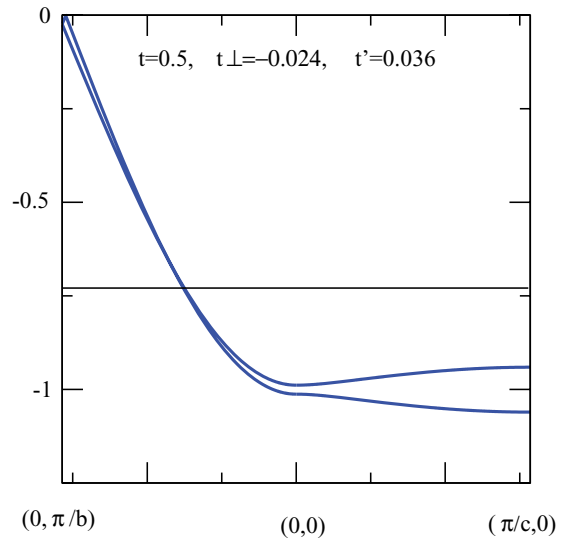


FIG. 2. (Color online) Band structure for the lower two bands obtained from the diagonalization of the 4×4 tight-binding matrix defined in the text using $t = 0.5$ eV, $t_{\perp} = -0.024$ eV, $t' = 0.036$ eV. These parameter values are chosen to produce band dispersions comparable to LDA-DFT calculations (Ref. 44). The band dispersions along the b and c directions are plotted. The horizontal line denotes the Fermi energy.

The final tight-binding 4×4 Hamiltonian to be diagonalized reads

$$H(k) = \begin{pmatrix} 0 & -t_{\perp} e^{ik \cdot \delta_{\perp}} & -2t' e^{ik \cdot \delta_1} \cos\left(\frac{\mathbf{k} \cdot \mathbf{b}}{2}\right) & -2t A(k_a, k_c) \cos\left(\frac{\mathbf{k} \cdot \mathbf{b}}{2}\right) \\ -t_{\perp} e^{-ik \cdot \delta_{\perp}} & 0 & -2t A(k_a, k_c) \cos\left(\frac{\mathbf{k} \cdot \mathbf{b}}{2}\right) & 0 \\ -2t' e^{-ik \cdot \delta_1} \cos\left(\frac{\mathbf{k} \cdot \mathbf{b}}{2}\right) & -2t A(k_a, k_c) \cos\left(\frac{\mathbf{k} \cdot \mathbf{b}}{2}\right) & 0 & -t_{\perp} e^{-ik \cdot \delta_{\perp}} \\ -2t A(k_a, k_c) \cos\left(\frac{\mathbf{k} \cdot \mathbf{b}}{2}\right) & 0 & -t_{\perp} e^{ik \cdot \delta_{\perp}} & 0 \end{pmatrix}.$$

In the absence of interladder hopping ($t' = 0$), the four bands

$$\epsilon(\mathbf{k}) = \pm t_{\perp} \pm 2t \cos\left(\frac{\mathbf{k} \cdot \mathbf{b}}{2}\right), \quad (12)$$

which recovers the expected dispersions of the uncoupled two-leg ladders, as it should.

Diagonalizing the Hamiltonian we obtain the band structure along the b and c directions shown in Fig. 2. The effective hopping between the nearest-neighbor Mo_1 - Mo'_4 atoms in a chain is taken to be $t = 0.5$ eV to reproduce the DFT bandwidth of the two lowest Mo d_{xy} energy bands. We use the hopping amplitudes $t' = 0.036$ eV a factor of 2 larger than the one obtained from Slater-Koster in Table II and we take the hopping between chains in the ladder opposite to t' and of magnitude $t_{\perp} = -0.024$ eV consistent with the type of bonding (π vs. δ bonding). This set of parameters captures the correct magnitude of the band dispersions along b , the dispersion of the two lowest bands in the c direction due to the combined coupling between ladders t' and the interchain hopping amplitude t_{\perp} . The magnitude of the values extracted from the present analysis t_{\perp} and t' of about 0.03 eV are consistent with recent preliminary estimates.²⁹

The Fermi surface obtained from the diagonalization of the 4×4 Hamiltonian is shown in Fig. 3. This tight-binding Fermi

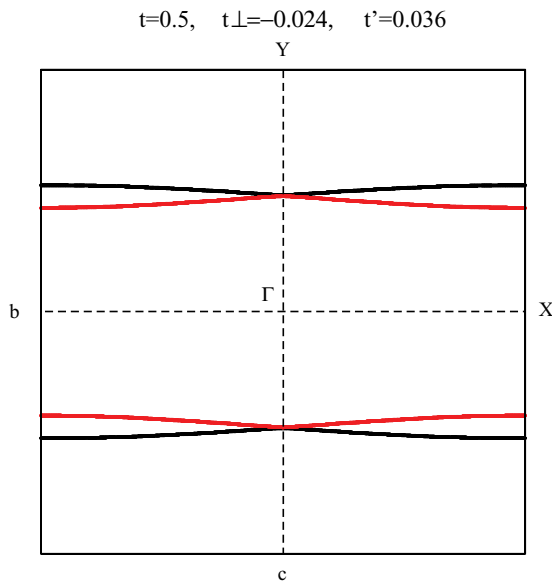


FIG. 3. (Color online) Fermi surface obtained from the diagonalization of the 4×4 matrix using $t = 0.5$ eV, $t_{\perp} = -0.024$ eV, $t' = 0.036$ eV, and filling $n = 1.9$. The Fermi sheets corresponding to the two separate bands are denoted in blue and red. Note that the two sheets have opposite warping.

surface is close to the DFT Fermi surface (cf. Fig. 6. in Ref. 44) except that the two Fermi sheets touch at the zone boundary in the DFT Fermi surface. The filling is $n = 1.9$, with the warping of the most-filled band opposite to the less-filled band. We note that the opposite signs of t' and t_{\perp} found in the Slater-Koster approach are essential for capturing the opposite warping of the two Fermi sheets found in DFT.

1. Fermi surface nesting instabilities

The tendency of the system towards nesting instabilities can be analyzed by computing the bare charge susceptibility,

$$\chi_{mm'}(\mathbf{q}) = \frac{2}{N} \sum_{\mathbf{k}} \frac{f(\epsilon_m(\mathbf{k} + \mathbf{q})) - f(\epsilon_{m'}(\mathbf{k}))}{\epsilon_m(\mathbf{k} + \mathbf{q}) - \epsilon_{m'}(\mathbf{k})}, \quad (13)$$

between the different bands $\epsilon_m(\mathbf{k})$. From a simple inspection of the Fermi surface in Fig. 3 one observes that since the two Fermi sheets corresponding to the two bands are oppositely warped the nesting condition is optimally satisfied with a nesting vector which is about $\mathbf{q} \approx (0, \pi/b, 0)$ between the two different bands. Evaluating $\chi_{mm'}(\mathbf{q})$ shown in Fig. 4, a divergence is observed in the interband susceptibility $\chi_{12}(\mathbf{q})$ when decreasing the temperature but not in the intraband contributions.

C. Quarter filling or half filling?

From a band-structure point of view the apparent half-filling arises because of the zig-zag structure of the chains which leads to a folding of the Brillouin zone. However, the key point (at least in terms of strong electronic correlations) is that for $\text{LiMoO}_6\text{O}_{17}$ there would be one electron per two Mo ions. In this sense the material should be viewed as being close to one-quarter filling. This is important because it means that long-range Coulomb interactions are required to produce an insulating state. We also note that both ARPES and LDA give

TABLE III. Estimates of the Coulomb and hopping parameters for $\text{Li}_{0.9}\text{Mo}_6\text{O}_{17}$. The on-site Coulomb repulsion U is obtained from constrained DFT calculations (Ref. 44). We have assumed $V = 2t$ appropriate for having the material in the proximity to a charge-order QCP (see Fig. 1). We have assumed a $1/d$ decay of the further off-diagonal Coulomb parameters with d , the distance between electrons in different sites. The Coulomb repulsion energies and hopping amplitudes in this table can be identified in the schematic structure of Fig. 5. All energies are given in eV.

t	t_{\perp}	t'	U	V	V_{\perp}	V'	V''	V'''	V''''
0.5	-0.024	0.036	6.4	1	1	0.7	0.66	0.65	0.53

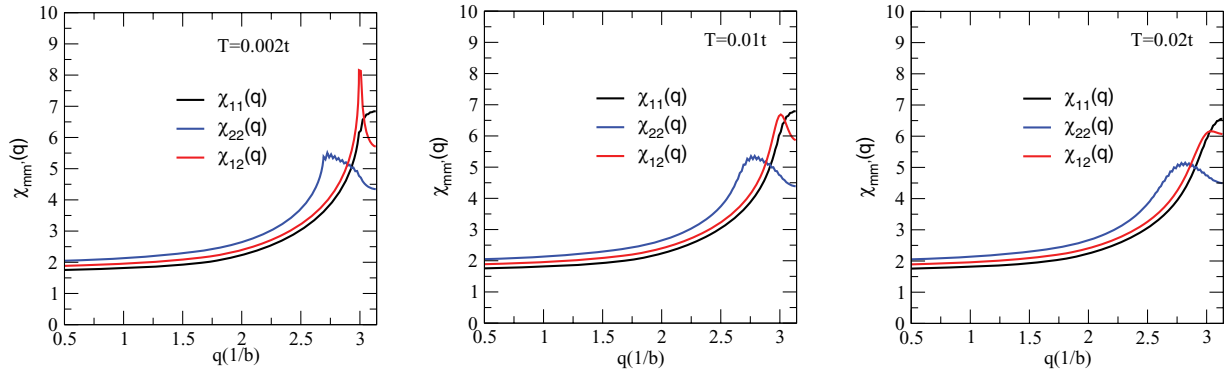


FIG. 4. (Color online) Wave-vector dependence of the three noninteracting charge susceptibilities. The three boxes correspond to decreasing temperature from left to right. The three susceptibilities are associated with the two low-energy bands crossing the Fermi surface and shown in Fig. 3 with $t = 0.5$ eV, $t_{\perp} = -0.024$ eV, $t' = 0.036$ eV, and filling $n = 1.9$. The interband susceptibility χ_{12} displays an instability at low temperatures due to significant nesting between these two Fermi sheets.

$k_F \simeq \pi/2b$ and this only corresponds to half-filling when b is the nearest-neighbor distance.

D. Anisotropy in the conductivity

In a simple Fermi liquid picture the ratio of the conductivity parallel and perpendicular to the chain directions is independent of temperature and given by

$$\frac{\sigma_b}{\sigma_a} \sim \left(\frac{t}{t'}\right)^2. \quad (14)$$

The estimates in Table III suggest an anisotropy ratio of about 100, which is consistent with that observed experimentally in Refs. 14, 13, and 15, but much larger than reported in Refs. 17 and 16.

IV. EFFECTIVE STRONGLY CORRELATED HAMILTONIAN

An effective Hamiltonian which can capture the electronic properties of $\text{Li}_{0.9}\text{MoO}_6\text{O}_{17}$ is now presented. We argue that since the system is close to quarter-filling not only the on-site U but also the off-site Coulomb repulsion V should be included to account for charge-ordering phenomena. This minimal model is an extended Hubbard model which reads

$$H = H_0 + H_U, \quad (15)$$

where H_0 is the noninteracting tight-binding Hamiltonian which reads

$$\begin{aligned} H_0 &= -t \sum_{\alpha,l,i\sigma} (c_{\alpha,i\sigma}^{(l)\dagger} c_{\alpha,i+1\sigma}^{(l)} + \text{c.c.}) - t_{\perp} \sum_{\alpha,l,i\sigma} (c_{\alpha,i\sigma}^{(l)\dagger} c_{\alpha,i\sigma}^{(l+1)} + \text{c.c.}) \\ &= -t' \sum_{\alpha,i\sigma} (c_{\alpha,2i-1\sigma}^{(l)\dagger} c_{\alpha+1,2i\sigma}^{(l+1)} + \text{c.c.}) \\ &\quad - t' \sum_{\alpha,i,\sigma} (c_{\alpha,2i+1\sigma}^{(l)\dagger} c_{\alpha+1,2i\sigma}^{(l+1)} + \text{c.c.}), \end{aligned} \quad (16)$$

where the first term describes the kinetic energy of a single ladder and the second term the hopping processes between ladders. The index l denotes one of the two chains in a ladder, α labels a specific ladder, and i runs from 1 to N , the number of sites in the chains. The parameters t , t_{\perp} ,

denote hopping amplitudes within a ladder whereas t' denotes the hopping amplitude connecting nearest-neighbor ladders. One only needs three hopping amplitude parameters for the description of the band structure. The Coulomb interactions are encoded in H_U , which reads

$$\begin{aligned} H_U &= U \sum_{\alpha,l,i\sigma} n_{\alpha i \uparrow}^{(l)} n_{\alpha i \downarrow}^{(l)} + V \sum_{\alpha,l,i} n_{\alpha,i}^{(l)\dagger} n_{\alpha,i+1}^{(l)} + V_{\perp} \sum_{\alpha,l,i} n_{\alpha,i}^{(l)} n_{\alpha,i}^{(l+1)} \\ &\quad + V' \sum_{\alpha,l,i} (n_{\alpha,i}^{(l)} n_{\alpha,i+1}^{(l+1)} + n_{\alpha,i+1}^{(l)} n_{\alpha,i}^{(l+1)}) + V'' \sum_{\alpha,l,i} n_{\alpha,i}^{(l)} n_{\alpha,i+2}^{(l)} \\ &\quad + V''' \sum_{\alpha,l,i} n_{\alpha,i}^{(l)} n_{\alpha+1,i+1}^{(l+1)} + V'''' \sum_{\alpha,l,i} n_{\alpha,i}^{(l)} n_{\alpha+1,i}^{(l+1)}. \end{aligned} \quad (17)$$

The parameters U , V , V_{\perp} , V' , and V'' denote intraladder Coulomb interactions, whereas V''' , V'''' , and V''''' denote Coulomb interactions between nearest-neighbor ladders. A schematic representation of the parameters entering the model proposed are displayed in Fig. 5. In principle, the model keeps the essential intraladder and interladder Coulomb repulsion energies that may be relevant for $\text{Li}_{0.9}\text{MoO}_6\text{O}_{17}$. Estimates of the values of Coulomb repulsion energies entering the Hamiltonian are provided and discussed below.

A. Model parameter values

In Table III we show the hopping amplitudes and Coulomb parameters estimated for model (15). From the comparison to the DFT-LDA calculations we found that the nearest-neighbor hopping is $t = 0.5$ eV, the hopping between chains in the same ladder is $t_{\perp} = -0.024$ eV, and between nearest-neighbor chains in different ladders $t' = 0.036$ eV. We note that for the case in which $t' = -3t_{\perp}/2$, we have that the two bands cross at $k_c = 0$ in agreement with the DFT calculations. When the same sign is used $t' = 3t_{\perp}/2$, then the two bands do not cross at $k_c = 0$. So it is essential that t_{\perp} and t' do have opposite signs to capture the appropriate warping and dispersions. The on-site Coulomb repulsion is about $U = 6.4$ eV estimated from constrained DFT⁴⁴ calculations.

The unscreened Coulomb interaction between electrons in nearest-neighbor Mo atoms within a chain is estimated to be $V = 2$ eV, which is comparable to the bandwidth and therefore relevant unless complete screening inside the crystal occurs.

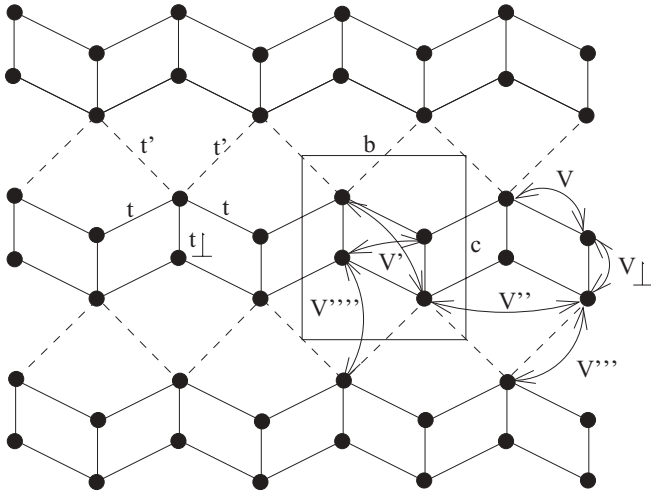


FIG. 5. Schematic representation of the model Hamiltonian (15) to describe $\text{Li}_{0.9}\text{Mo}_6\text{O}_{17}$. The hopping and Coulomb energies entering the model describing electrons in the d_{xy} orbitals of Mo are displayed. A schematic view perpendicular to the b - c plane is shown noting that the planes of the ladders in the real crystal are tilted with respect to the b - c plane. The rectangle corresponds to the unit cell in the b - c plane.

These values are large enough to lead to charge-ordered ground states since the critical value V_c in a quarter-filled chain is about $V \approx 2t$. Screened values of V are reduced to about $V = 0.2$ eV, assuming a dielectric constant of $\epsilon \approx 10\epsilon_0$ due to the screening of the rest of the crystal.⁴⁴

In a similar quarter-filled ladder⁵⁶ compound NaV_2O_5 charge-ordering phenomena due to the off-site Coulomb repulsion has been found. From DFT-based calculations the parameters are estimated to be $t_{\parallel} \simeq 0.17$ eV, $t_{\perp} \simeq 3t$, and $U \simeq 2.8$ eV. The distance between vanadium ions along the chain is approximately 3.8 Å and the nearest-neighbor Coulomb repulsion V has been estimated⁵⁷ to be $V \approx 2t$ consistent with the zig-zag type charge ordering⁵⁸ found in these systems.

Experimental observations combined with the present discussion suggest that in $\text{Li}_{0.9}\text{Mo}_6\text{O}_{17}$, it is desirable that the Coulomb repulsion $V \sim 0.5$ – 1 eV so that the system is placed near the QCP to a charge-order transition driven by V (cf. Fig. 1). This requires that the long-range Coulomb repulsion is only partially screened and is important to understand the electronic properties of $\text{Li}_{0.9}\text{Mo}_6\text{O}_{17}$. The relevance of incomplete Coulomb screening to the electronic properties of quasi-one-dimensional systems has already been pointed out in the case of tetrathiafulvalene-tetracyanoquinodimethane (TTF-TCNQ)^{59,60} crystals.

We now discuss the relevance of further neighbor Coulomb interactions. The Coulomb repulsion between chains in the same ladder should be similar to the nearest-neighbor V since the distance between two neighboring Mo atoms in the same chain is 3.725 Å and is 3.675 Å between atoms in different chains, so $V_{\perp} \approx V$. This parameter is important for stabilizing a zig-zag type of charge-ordered state in the ladder. Comparing the distances between different Mo atoms one realizes that further neighbor interactions are relevant to the model. In fact,

the Coulomb repulsion between electrons on Mo atoms on different zig-zag chains of the same ladder (see Fig. 5), V' is comparable to V and V_{\perp} since interladder distances are between 5.256 and 5.366 Å. Since the next-nearest-neighbors distance between two Mo is 5.52 Å due to the zig-zag nature of the chains, we have that V'' is not negligible. On the other hand, the nearest distance between Mo atoms in nearest ladders is 5.77 Å so the Coulomb repulsion between neighboring ladders V''' is comparable to V'' . The off-site Coulomb repulsion included in the model is cutoff at values of the Coulomb repulsion at which $V'''' \sim V/2 \sim t$, assuming $V \sim 2t$. Coulomb energies between farther distant neighbors are neglected since they are smaller than the bare kinetic energy of the electrons.

Hence, a minimal model should contain the nearest-neighbor Coulomb interactions and possibly longer-range Coulomb interactions between electrons in further distant Mo atoms as represented in Fig. 5. Accurate screening calculations in $\text{Li}_{0.9}\text{Mo}_6\text{O}_{17}$ should be performed to pin down the values of the off-site Coulomb repulsion and settle the relevance of the longer-range Coulomb repulsion in $\text{Li}_{0.9}\text{Mo}_6\text{O}_{17}$. Similar conclusions have been reached based on estimates of the Coulomb screening energy.⁶¹ Below we discuss the minimal strongly correlated model (15) in some specific limits for which there are known results.

The estimated hoppings and Coulomb parameters of the model are summarized in Table III.

V. UNDERSTANDING THE MODEL HAMILTONIAN

In principle, the model (15) is effectively two dimensional consisting of zig-zag ladders which are weakly coupled through t' and there is also Coulomb repulsion between electrons in different ladders. The relevance of the interladder hopping interactions is settled by the temperature scale at which actual experiments are undertaken. As a first step in the understanding of the full complexity of the model we discuss the physics of isolated chains and ladders for which much more theoretical work is available. Therefore, we first consider the model (15) in different limits assuming independent ladders ($t' = 0$ and $V''' = V'''' = 0$) so we are left only with t , t_{\perp} , and the Coulomb repulsion energies U , V , V_{\perp} , and V' .

A. What is the ground state of the ladder model at one-quarter filling and $U \rightarrow \infty$?

We consider quarter-filled ladders assuming that doubly occupied sites are forbidden ($U \rightarrow \infty$). This model has been studied numerically using density matrix renormalization group (DMRG)⁶² and analytically through weak coupling RG and bosonization techniques⁶³ in different parameter ranges which we now discuss.

1. $t_{\perp} = V_{\perp} = V' = 0$

The two chains comprising the ladder are completely decoupled and the model maps onto the t - V model of spinless fermions at half-filling. The ground state is a Luttinger liquid for $V < 2t$ and an insulator with long-range charge order for $V > 2t$ (Ref. 64). Even in the presence of the long-range

Coulomb interaction decaying as $1/d$, where d is the distance between electrons in different sites, it is found that the Wigner state with one electron at every other site of the lattice is the ground state at one-quarter filling⁵⁹ when $t \rightarrow 0$. This is satisfied in this case indicating that charge-ordered states are nonfrustrated by the longer-range part of the Coulomb interaction. Also recent DMRG calculations on two-leg ladders with $t_{\perp} = t$ show an insulating phase with a charge gap which is interpreted as a result of dimerization of the rungs with one electron localized on each rung of the ladder.⁶⁵

2. $t_{\perp} = V' = 0, V_{\perp} \neq 0$

This ladder model has been studied by bosonization and RG approaches.⁶³ There are two charge modes, total and difference. For $0 < V < 2t$, the difference mode can be gapless. The other is gapped in the presence of a small V_{\perp} . This is a homogeneous insulating phase consistent with DMRG results performed for $t_{\perp}/t < 1$ (Ref. 62). When both $V = V_{\perp} > 2t$ the insulating phase has zig-zag charge order with wave vector (π, π) . The role of V_{\perp} is crucial in locking the charge-order waves running along the two independent chains when these are decoupled. Interestingly, even at $V = 0$ and for any finite V_{\perp} the system displays a charge gap which has an exponential dependence with V_{\perp} as in the half-filled Hubbard model leading to a homogeneous insulator.

3. $V' \neq 0$

This interaction frustrates charge order and should produce a metallic state when $V' \sim V \sim V_{\perp}$, even when $V \gg t$ (Ref. 66). In this limit, the model can be mapped onto a classical Ising model with frustrated interactions which leads to a disordered ground state. A quarter-filled one-dimensional extended model⁶⁷ with nearest, V , and next-nearest Coulomb interactions, V' has been analyzed using DMRG which shows a metallic state when $V' \sim V/2$.

B. Triplet superconductivity

Quantum Monte Carlo calculations on a nearly quarter-filled model of weakly coupled chains with on-site Coulomb repulsion interaction U only and small $U = 2t$ display f -wave (spin triplet) superconducting tendencies due to $2k_f$ -CDW instabilities. The f -wave symmetry is related to the fact that the electronic modulation is of about four lattice spacings $Q \approx 2k_f \approx \pi/2$ close to quarter-filling.⁶⁸ Such behavior has been confirmed by a random phase approximation (RPA) analysis in weakly coupled quarter-filled chains with Coulomb interactions up to third nearest neighbors in the presence of interchain Coulomb repulsion.⁶⁹ It is found that for $U = 1.7t$, $t_{\perp} = 0.2t$, and under the condition $V' + V_{\perp} \approx U/2$, triplet f -wave superconductivity wins over the d -wave channel. This is because the presence of V_{\perp} enhances the $2k_f$ -CDW instabilities of the isolated chains. Triplet superconductivity pairing has also been encountered in weak coupling RG calculations on weakly coupled chains in the presence of both intrachain and interchain Coulomb repulsion⁷⁰ for moderate values of the interchain Coulomb repulsion.

For the two-dimensional quarter-filled extended Hubbard model it is found that introducing frustrating charge interac-

tions on the square lattice (e.g., along one diagonal) destabilizes the stripe charge-ordered insulating phases producing a charge-ordered 3-fold symmetric metallic state⁷¹ at large V and at finite U . In the limit of $U \gg t$ a metallic “pinball” liquid state in which no doubly occupied sites (“pins”) can occur.^{12,72} Melting the 3-fold state produces an “ f -wave” spin triplet superconducting state. How this particular symmetry emerges can be seen from direct inspection of the 3-fold charge-ordering pattern in real space which consists of placing electrons on the closest sites not coupled via the Coulomb interaction to a given occupied site, avoiding the off-site Coulomb repulsion. Thus, the f -wave pairing found in the isotropic triangular lattice is analogous to the d_{xy} -wave pairing found on the square lattice³⁴ and results from electrons avoiding the strongest nearest-neighbor Coulomb repulsion.

C. Doping the ladder away from one-quarter filling

Since $\text{Li}_{0.9}\text{Mo}_6\text{O}_{17}$ is slightly doped away from one quarter-filling it is worth considering this situation. Assuming that $t_{\perp} = V' = 0$ and $V_{\perp} \neq 0$ as above there is a metallic state if the chemical potential is of the order of the gap of the quarter-filled system⁶³ based on weak coupling RG. This is because a commensurate-incommensurate transition occurs since Umklapp processes are suppressed as $4k_f \neq |\mathbf{G}|$ where \mathbf{G} is a reciprocal vector of the lattice. On the other hand, superconducting fluctuations in the doped quarter-filled ladder are found to be of the singlet d -wave type but dominated by the $4k_f$ -CDW correlations. However, including longer-range Coulomb interactions can change this picture and induce f -wave triplet pairing. It remains an open question to understand how the presence of V' can influence the superconducting tendencies of the system in ladders doped away from quarter-filling.

VI. CONCLUSION

The title quasi-one-dimensional material displays an intriguing competition between insulating, superconducting, and “bad” metallic behavior. Besides the mechanism of superconductivity, the nature of the “insulating” phase and the unconventional metallic properties are poorly understood. No evidence of a structural transition has been found accompanying the occurrence of the “insulating” phase. Under pressure the insulating phase is suppressed giving way to conventional metallic behavior below a low-temperature crossover scale.

To understand these phenomena, we have derived a minimal strongly correlated model for determining the low-energy electronic properties of $\text{Li}_{0.9}\text{Mo}_6\text{O}_{17}$. The one-electron part of the Hamiltonian is obtained based on a Slater-Koster approach and comparison to DFT band-structure calculations. The tight-binding Hamiltonian consists of three hopping parameters only: t , t_{\perp} , and t' , which capture the dispersion of the two $\text{Mo}(d_{xy})$ bands along the b direction crossing the Fermi energy, the opposite warping of the two Fermi surface sections, and the weak dispersion of the two bands in the c direction. These are the main features found in full band-structure calculations. The real-space tight-binding Hamiltonian describes zig-zag ladders weakly coupled by the small interladder hopping t' . In the lattice model we note that the system is close to quarter-filling

although the bands are nearly half-filled. This is a result of the band folding associated with the four atoms in the unit cell arising from the zig-zag structure of the ladders.

A reinterpretation of the physics of $\text{Li}_{0.9}\text{Mo}_6\text{O}_{17}$ as a nearly quarter-filled system instead of a nearly half-filled system is suggested from the model introduced. Both the on-site U and off-site Coulomb repulsion beyond the nearest neighbors are found to be relevant since estimated values can be comparable to the bandwidth of the material. Based on these estimates and experiments under pressure we suggest that $\text{Li}_{0.9}\text{Mo}_6\text{O}_{17}$ is close to a charge-ordering transition driven by the Coulomb repulsion. Based on the sensitivity of the material to external pressure we argue that many of the anomalies observed may arise due to the proximity to a quantum critical point (QCP). The “bad” metal behavior is attributed to quantum criticality: a metal with unconventional excitations arising from the charge fluctuations occurring at all length scales around the QCP. Associated with the QCP is the existence of a crossover temperature T^* below which coherent excitations and Fermi liquid behavior occurs on the metallic side of the transition. This scale is suppressed as the QCP is approached. Quantum fluctuations associated with charge order occur in the proximity to the QCP which can lead to the enhancement in the resistivity below T_m leading to a resistivity minimum which has been found in other quasi-one-dimensional materials close to CDW instabilities, such as $\text{Per}_2\text{M}(\text{mnt})_2$ [$\text{M} = \text{Pt}, \text{Au}$] (Ref. 36).

Spin triplet superconductivity can arise in systems in which charge fluctuations associated with a nearby charge-ordered phase dominate. In general, in ladder systems explored close to quarter-filling, zig-zag charge order correlations are strongly

enhanced even by moderate interchain Coulomb repulsion V_\perp , as previous works have shown. In $\text{Li}_{0.9}\text{Mo}_6\text{O}_{17}$, the fact that $V_\perp = V$ and the presence of next-nearest neighbors Coulomb interaction and longer-range interactions along the chains due to the zig-zag structure can favor spin triplet superconductivity.

Experiments probing the existence of large charge fluctuations near the QCP are desirable to understand the enhancement of the resistivity with decreasing temperature. X-ray diffraction finds no structural changes associated with the upturn of the resistivity at T_m suggesting that a purely electronic mechanism plays a major role. From the T dependence of the $1/T_1T$ -NMR spectra one could find whether anomalous broadening or splitting of spectral lines⁷³ occurs when lowering the temperature below T_m in analogy to $\text{TMTTF}_2\text{AsF}_6$ (Ref. 74), in which the charge-ordering transition detected by NMR is not accompanied by a change of the structure. This kind of experiment could clarify the role played by charge-ordering phenomena driven by the off-site Coulomb repulsion as proposed here.

ACKNOWLEDGMENTS

We thank Nigel Hussey for stimulating our interest in this material and for many helpful discussions. J. M. thanks J. V. Álvarez for helpful insights. R.M. received financial support from an Australian Research Council Discovery Project Grant No. DP0877875. J. M. acknowledges financial support from the International Collaboration Agreement from Australian Research Council Discovery Project (DP10932249) [Chief Investigator: B.J. Powell] and Ministerio de Economía y Competitividad in Spain (MAT2011-22491).

*jaime.merino@uam.es

†r.mckenzie@uq.edu.au

¹T. Giamarchi, *Chem. Rev.* **104**, 5037 (2004).

²B. J. Kim, H. Koh, E. Rotenberg, S.-J. Oh, H. Eisaki, N. Motoyama, S. Uchida, T. Tohyama, S. Maekawa, and Z.-X. Shen, *Nat. Phys.* **2**, 397 (2006).

³T. E. Kidd, T. Valla, P. D. Johnson, K. W. Kim, G. D. Gu, and C. C. Homes, *Phys. Rev. B* **77**, 054503 (2008).

⁴R. Claessen, M. Sing, U. Schwingenschlogl, P. Blaha, M. Dressel, and C. S. Jacobsen, *Phys. Rev. Lett.* **88**, 096402 (2002).

⁵M. Bockrath *et al.*, *Nature (London)* **397**, 598 (1999).

⁶H. Ishii *et al.*, *Nature (London)* **426**, 540 (2003).

⁷O. M. Auslaender *et al.*, *Science* **308**, 88 (2005).

⁸Y. Jompol *et al.*, *Science* **325**, 597 (2009).

⁹C. Blumenstein *et al.*, *Nat. Phys.* **7**, 776 (2011).

¹⁰F. Wang, J. V. Alvarez, S. K. Mo, J. W. Allen, G. H. Gweon, J. He, R. Jin, D. Mandrus, and H. Hochst, *Phys. Rev. Lett.* **96**, 196403 (2006).

¹¹C. Escribe Filippini *et al.*, *Physica C* **162–164**, 427 (1989).

¹²L. Cano-Cortés, J. Merino, and S. Fratini, *Phys. Rev. Lett.* **105**, 036405 (2010).

¹³J. F. Mercure, A. Bangura, X. Xu, N. Wakeham, A. Carrington, P. Walmsley, M. Greenblatt, and N. Hussey, *Phys. Rev. Lett.* **108**, 187003 (2012).

¹⁴X. Xu *et al.*, *Phys. Rev. Lett.* **102**, 206602 (2009).

¹⁵N. Wakeham *et al.*, *Nature Comm.* **2**, 396 (2011).

¹⁶H. Chen *et al.*, *Europhys. Lett.* **89**, 67010 (2010).

¹⁷M. S. da Luz, C. A. M. dos Santos, J. Moreno, B. D. White, and J. J. Neumeier, *Phys. Rev. B* **76**, 233105 (2007).

¹⁸J. Merino and R. H. McKenzie, *Phys. Rev. B* **61**, 7996 (2000).

¹⁹O. Gunnarsson, M. Calandra, and J. E. Han, *Rev. Mod. Phys.* **75**, 1085 (2003).

²⁰N. H. Lindner and A. Auerbach, *Phys. Rev. B* **81**, 054512 (2010).

²¹N. E. Hussey, K. Takenaka, and H. Takagi, *Phil. Mag.* **84**, 2847 (2004).

²²M. Boujida *et al.*, *Physica C* **153–155**, 465 (1988).

²³J. L. Cohn, B. D. White, C. A. M. dos Santos, and J. J. Neumeier, *Phys. Rev. Lett.* **108**, 056604 (2012).

²⁴K. Behnia *et al.*, *J. Phys.: Cond. Matter* **16**, 5187 (2004).

²⁵J. Choi, J. L. Musfeldt, J. He, R. Jin, J. R. Thompson, D. Mandrus, X. N. Lin, V. A. Bondarenko, and J. W. Brill, *Phys. Rev. B* **69**, 085120 (2004).

²⁶In a quasi-one-dimensional system band structure effects leads to a modified Drude expression⁷⁵: $R_H = \frac{\beta}{n|e|}$, where $\beta = -\frac{k_F}{v_F} \frac{\partial^2 \epsilon(k_F)}{\partial k_b^2}$, with $v_F = |\frac{\partial \epsilon(k_F)}{\partial k_b}|$ and k_F the Fermi wavevector. In a quasi-one-dimensional crystal with dispersion: $\epsilon(k_b) = -2t \cos(k_b b/2)$, ($t > 0$) appropriate for the Bechgaard salts: $(\text{TMTSF})_2\text{X}$, the simple Drude expression is modified to: $R_H = -\frac{1}{n|e|} \frac{k_F b/2}{\tan(k_F b/2)}$, where

- $b/2$ is the lattice constant along the chain direction.^{76,77} For $k_F = \frac{\pi}{2b}$ relevant to $\text{Li}_{0.9}\text{Mo}_6\text{O}_{17}$, we have $R_H = -\frac{\pi}{4} \frac{1}{n|e|} < 0$.
- ²⁷B. Korin-Hamzic, E. Tafra, M. Basletic, A. Hamzic, and M. Dressel, *Phys. Rev. B* **73**, 115102 (2006).
- ²⁸G. León, C. Berthod, and T. Giamarchi, *Phys. Rev. B* **75**, 195123 (2007).
- ²⁹F. Wang, J. V. Alvarez, J. W. Allen, S. K. Mo, J. He, R. Jin, D. Mandrus, and H. Hochst, *Phys. Rev. Lett.* **103**, 136401 (2009).
- ³⁰V. Meden and K. Schönhammer, *Phys. Rev. B* **46**, 15753 (1992).
- ³¹J. Voit, *Phys. Rev. B* **47**, 6740 (1993).
- ³²J. Hager, R. Matzdorf, J. He, R. Jin, D. Mandrus, M. A. Cazalilla, and E. W. Plummer, *Phys. Rev. Lett.* **95**, 186402 (2005).
- ³³K. Behnia, *J. Phys.: Cond. Matter* **21**, 113101 (2009).
- ³⁴J. Merino and R. H. McKenzie, *Phys. Rev. Lett.* **87**, 237002 (2001).
- ³⁵H. Nishikawa, Y. Sato, K. Kikuchi, T. Kodama, I. Ikemoto, J. Yamada, H. Oshio, R. Kondo, and S. Kagoshima, *Phys. Rev. B* **72**, 052510 (2005).
- ³⁶N. Mitsu *et al.*, *J. Phys. Chem. Solids* **66**, 1567 (2005).
- ³⁷G. Grüner, *Density Waves in Solids* (Addison-Wesley, Reading, MA, 1994).
- ³⁸M. S. da Luz, J. J. Neumeier, C. A. M. dos Santos, B. D. White, H. J. I. Filho, J. B. Leao, and Q. Huang, *Phys. Rev. B* **84**, 014108 (2011).
- ³⁹C. A. M. dos Santos, B. D. White, Y. K. Yu, J. J. Neumeier, and J. A. Souza, *Phys. Rev. Lett.* **98**, 266405 (2007).
- ⁴⁰K. Maki, B. Dora, M. Kartsovnik, A. Virosztek, B. Korin-Hamzic, and M. Basletic, *Phys. Rev. Lett.* **90**, 256402 (2003).
- ⁴¹S. Chakravarty, R. B. Laughlin, D. K. Morr, and C. Nayak, *Phys. Rev. B* **63**, 094503 (2001).
- ⁴²Y. Matsuda, M. Sato, M. Onoda, and K. Nakao, *J. Phys. C* **19**, 6039 (1986).
- ⁴³C. Schlenker, H. Schwenk, C. Escribe-Filippini, and J. Marcus, *Physica B + C* **135**, 511 (1985).
- ⁴⁴Z. S. Popovic and S. Satpathy, *Phys. Rev. B* **74**, 045117 (2006).
- ⁴⁵R. H. McKenzie, [arXiv:cond-mat/9905044v2](https://arxiv.org/abs/cond-mat/9905044v2).
- ⁴⁶B. J. Powell and R. H. McKenzie, *Phys. Rev. B* **69**, 024519 (2004), and references therein.
- ⁴⁷M. Whangbo, E. Canadell, and C. Schlenker, *J. Am. Chem. Soc.* **109**, 6308 (1987).
- ⁴⁸M. Whangbo, E. Canadell, P. Foury, and J.-P. Pouget, *Science* **252**, 96 (1991).
- ⁴⁹C. Escribe Filippini *et al.*, *Phil. Mag. B* **50**, 321 (1984).
- ⁵⁰P.-A. Glans, T. Learmonth, K. E. Smith, T. Valla, P. D. Johnson, S. L. Hulbert, W. McCarroll, and M. Greenblatt, *Phys. Rev. B* **72**, 035115 (2005).
- ⁵¹M. Whangbo and E. Canadell, *J. Am. Chem. Soc.* **110**, 358 (1988).
- ⁵²J. C. Slater and G. F. Koster, *Phys. Rev.* **94**, 1498 (1954).
- ⁵³W. A. Harrison, *Electronic Structure and the Properties of Solids* (Dover, New York, 1989).
- ⁵⁴M. Onoda *et al.*, *J. Solid State Chem.* **66**, 163 (1987).
- ⁵⁵T. Jarlborg, P. Chudzinski, and T. Giamarchi, *Phys. Rev. B* **85**, 235108 (2012).
- ⁵⁶H. Smolinski, C. Gros, W. Weber, U. Peuchert, G. Roth, M. Weiden, and C. Geibel, *Phys. Rev. Lett.* **80**, 5164 (1998).
- ⁵⁷A. Bernert, T. Chatterji, P. Thalmeier, and P. Fulde, *Eur. Phys. J. B* **21**, 535 (2001).
- ⁵⁸B. Edegger, H. G. Evertz, and R. M. Noack, *Phys. Rev. Lett.* **96**, 146401 (2006).
- ⁵⁹J. Hubbard, *Phys. Rev. B* **17**, 494 (1978).
- ⁶⁰L. Cano-Cortés *et al.*, *Eur. Phys. J. B* **56**, 173 (2007).
- ⁶¹P. Chudzinski, T. Jarlborg, and T. Giamarchi, [arXiv:1205.0239v1](https://arxiv.org/abs/1205.0239v1).
- ⁶²M. Vojta, A. Hubsch, and R. M. Noack, *Phys. Rev. B* **63**, 045105 (2001).
- ⁶³E. Orignac and R. Citro, *Eur. Phys. J. B* **33**, 419 (2003).
- ⁶⁴S. Nishimoto and M. Tsuchiizu, *Phys. Rev. B* **81**, 085116 (2010).
- ⁶⁵L. Liu, H. Yao, E. Berg, and S. A. Kivelson, *Phys. Rev. Lett.* **108**, 126406 (2012).
- ⁶⁶H. Seo, K. Tsutsui, M. Ogata, and J. Merino, *J. Phys. Soc. Jpn.* **75**, 114707 (2006).
- ⁶⁷S. Ejima, F. Gebhard, S. Nishimoto, and Y. Ohta, *Phys. Rev. B* **72**, 033101 (2005).
- ⁶⁸K. Kuroki, Y. Tanaka, T. Kimura, and R. Arita, *Phys. Rev. B* **69**, 214511 (2004).
- ⁶⁹K. Kuroki and Y. Tanaka, *J. Phys. Soc. Jpn.* **74**, 1694 (2005).
- ⁷⁰J. C. Nickel, R. Duprat, C. Bourbonnais, and N. Dupuis, *Phys. Rev. Lett.* **95**, 247001 (2005).
- ⁷¹H. Watanabe and M. Ogata, *J. Phys. Soc. Jpn.* **74**, 2901 (2005).
- ⁷²C. Hotta and N. Furukawa, *Phys. Rev. B* **74**, 193107 (2006).
- ⁷³K. Hiraki and K. Kanoda, *Phys. Rev. Lett.* **80**, 4737 (1998).
- ⁷⁴D. S. Chow, F. Zamborszky, B. Alavi, D. J. Tantillo, A. Baur, C. A. Merlic, and S. E. Brown, *Phys. Rev. Lett.* **85**, 1698 (2000).
- ⁷⁵V. M. Yakovenko and A. T. Zheleznyak, *Synth. Met.* **103**, 2202 (1999).
- ⁷⁶J. R. Cooper *et al.*, *J. Phys. (France)* **38**, 1097 (1977).
- ⁷⁷A. Virosztek and K. Maki, *Phys. Rev. B* **39**, 616 (1989).